IEEE Access
Multidisciplinary | Rapid Review | Open Access Journal

Received 11 August 2022, accepted 2 September 2022, date of publication 12 September 2022, date of current version 5 October 2022.

Digital Object Identifier 10.1109/ACCESS.2022.3206091

RESEARCH ARTICLE

Risk-Aware Energy Management for Drive Mode Control in Plug-in Hybrid Electric Vehicles

RYUNOSUKE WATANABE[1], (Member, IEEE), TATSUYA IBUKI[2], (Member, IEEE), YOSHIHIRO SAKAYANAGI[3], RIKU FUNADA[1], (Member, IEEE), AND MITSUJI SAMPEI[1], (Member, IEEE)

[1]Tokyo Institute of Technology, Tokyo 152-8550, Japan
[2]School of Science and Technology, Meiji University, Kawasaki City, Kanagawa 214-8571, Japan
[3]Toyota Motor Corporation, Susono City, Shizuoka 410-1193, Japan

Corresponding author: Ryunosuke Watanabe (rwata@sl.sc.e.titech.ac.jp)

This work was supported by the Japan Science and Technology Agency (JST) Support for Pioneering Research Initiated by the Next Generation (SPRING) under Grant JPMJSP2106.

This work involved human subjects or animals in its research. Approval of all ethical and experimental procedures and protocols was granted by the Tokyo Institute of Technology's Human Subjects Research Ethics Review Committee.

ABSTRACT This paper proposes risk-aware energy management for drive mode control in plug-in hybrid electric vehicles (PHEVs) to reduce fuel consumption. This paper focuses on reducing fuel usage in scenarios in which energy demands along a planned route are stochastically estimated using historical driving data. In this scenario, the proposed method evaluates the risk of high energy consumption based on the conditional value at risk (CVaR) and entropic value at risk (EVaR) derived from Chernoff's inequality. The CVaR quantifies the high fuel consumption expected in the tail of the probability distributions as a cost function. In contrast, the EVaR bound constraint provides stochastic constraints of electricity capacity based on the property of the cumulant-generating function. Each risk evaluation is formulated as a mixed-integer exponential cone programming problem by expressing the drive modes of a PHEV as binary variables. The proposed method was demonstrated using a detailed vehicle simulator with real-world driving cycles. The designed controller achieved, on two selected routes, 8.60% and 16.09% improvements on average, and 10.75% and 12.85% reductions at the 75th percentile compared to a commercial method. The simulations indicated that we can design the controller characteristics by adjusting the risk-awareness of energy loss. The conservativeness of the risk evaluation is also discussed based on the simulation results.

INDEX TERMS Energy management, optimization-based control, plug-in hybrid electric vehicles, risk measurement.

I. INTRODUCTION

Energy management strategies for plug-in hybrid electric vehicles (PHEVs) have been studied extensively [1], [2], [3]. These strategies have also been discussed mathematically as an energy allocation problem. For PHEVs, automobiles generate driving power by consuming fuel or electricity from energy resources. The characteristics of the resources vary depending on the driving states of the mechanisms, e.g., combustion engine, storage systems, gears, and wheels. To achieve a desirable fuel economy under these characteristics, researchers have proposed statistical data-base power train control and energy allocation methods in recent years [4], [5], [6], [7].

Commercial PHEVs adopt a rule-based method called the charge-depleting and charge-sustaining (CDCS) method because of its simplicity. The CDCS rule is as follows: 1) depleting stored electricity from a battery; 2) consuming fuel to cruise the remaining course and sustain a state of charge (SoC) of the battery. The CDCS method is not optimal in terms of fuel economy when the battery capacity is less than the required energy for the entire travel [8].

The associate editor coordinating the review of this manuscript and approving it for publication was Mauro Gaggero.

This simple rule-based method has been used because of the lack of computational resources.[1] This computing environment is improving, and management systems can now utilize statistical information. In [4], [9], and [10] employing dynamic programming as a model-based optimization, finite-horizon prediction enabled online calculations. The finite-horizon control method has a tradeoff between computational burden and performance, i.e., the horizon length. In [11], [12], and [13], dynamic programming-based energy management approaches were developed by assessing measured cycle data. These methods model the most representative trip based on measured data and predict the power demands of a vehicle. The representative trip model approximates the energy consumption of long distances as deterministic values, facilitating long-sighted management. Driver-aware vehicle control methods for hybrid electric vehicles have also been proposed. Driver behaviors are modeled as a Markov chain for scenario-based stochastic model predictive control (MPC) [6] or a multi-objective optimization framework [14]. The optimization method provides a personalized controller for the driver while considering driving conditions. In [15], [16], [17], and [18], traffic data-driven predictive control frameworks were developed, and the methods achieved near-optimal fuel consumption. As more advanced strategies utilize traffic data, some energy management systems can access real-time information containing vehicle speed, terrain, and infrastructure via vehicle-to-vehicle (V2V) and vehicle-to-cloud (V2C) connection technology [19], [20]. The V2V- and V2C-based methods model and observe traffic data and traffic light information to infer the energy consumption in real time. Because this method obtains a large amount of data, it is also highly compatible with machine learning, which is constantly evolving. References [17], [21] used machine learning techniques to avoid complex numerical optimization. Our previous studies [22], [23] presented a method for utilizing historical driving data and verified its effectiveness through experiments. The experiments showed that the proposed approach achieves a 15.9% improvement on average compared with the CDCS method.

The above-mentioned approaches utilize statistical information such as human behavior and environments. These methods belong to the class of stochastic control methods. More recently, because a large amount of data can be collected, risk-aware methods have received considerable interest [24], [25], [26], [27], [28], [29]. Risk-aware control and management have been widely discussed and accepted in finance and operations research [30], [31]. For quantifying the risk measure, high-order moments and cumulants and the conditional value at risk (CVaR) are considered in [24], [30], [32], [33], and [34]. The studies [33], [34] analyzed cost-cumulant control for continuous- and discrete-time linear-quadratic problems. A stochastic optimal control problem motivated by human behavior was studied in [25], and the study validated the approach through an experiment using a robot manipulator. The research [30] addressed an optimal control problem involving the CVaR in a discrete-time and discrete-state Markov decision process setting. As an application of the CVaR cost control method, real-time scheduling of residential appliances was presented by [35]. The analysis in [28] examined CVaR safety using recently developed control barrier functions. A risk-sensitive motion planning method was provided in [29]. This method embraces the entropic value at risk (EVaR), which is an upper bound on the CVaR and value at risk (VaR). The CVaR and EVaR used in these previous studies are closely related to convex optimization and are compatible with optimization-based control.

This paper explores the risk measure characteristics of statistical data and proposes risk-aware energy management for drive mode switching in PHEVs. The proposed method evaluates the risk of energy loss using CVaR cost and EVaR-bound constraints that were not considered in our previous method [22], [23]. The CVaR quantifies heavy fuel consumption events and can prevent the spread of the probability distribution in the positive direction. The EVaR can numerically provide a less conservative bound for the stochastic constraint of the sum of random variables. This is because the EVaR bound has high-order cumulants defined by the cumulant-generating function. The CVaR-based cost function and EVaR-based stochastic constraint enable us to formulate a one-stage mixed-integer exponential cone programming (MIECP) problem with a disciplined convex programming framework. The decision variables are the drive mode inputs for minimizing fuel consumption. The main contributions of this study are as follows: 1) Deriving a stochastic constraint formulation with the EVaR in terms of Chernoff's inequality. 2) Formulate an MIECP problem to evaluate the energy loss risk to determine optimal vehicle threshold values on which the PHEVs select the drive mode. 3) Analysis of the properties of the proposed method through numerical simulations using a detailed vehicle simulator called ADVISOR [36] with real-world data.

The remainder of this paper is organized as follows: Section II explains some preliminaries to provide the main result for the proposed method. Section III provides driving-route and vehicle modeling with updates from our previous paper [22], [23]. Section IV defines the cost function and the stochastic constraints and then proposes risk-aware energy management for the drive mode switching. Section V demonstrates the effectiveness of the proposed method and analyzes the sensitivity of the design parameters. The conclusions are discussed in Section VI.

II. PRELIMINARIES

This section provides some preliminaries to derive the main results of risk-aware energy management for drive mode switching. The preliminaries indicate the properties of the tail distributions for a random variable X. These properties enable us to assess the tail values of the probability distribution as risk measures.

[1] Another reason is that fuel economy assessments on PHEVs in most countries assume the CDCS method.

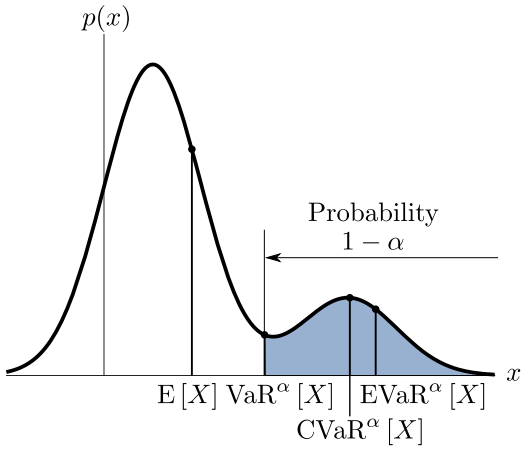

FIGURE 1. Relation to the expected value, VaR, CVaR, and EVaR for a given confidence level $\alpha \in [0, 1)$: The graph denotes a probability density function $p(x)$. The filled area denotes the $1-\alpha$% of the area under $p(x)$.

Notation: $\mathbb{R}$ is the set of real numbers. $\mathrm{E}[\cdot]$ ($\mathrm{E}[\cdot|\cdot]$) denotes the (conditional) expected value operator. $\Pr[\cdot]$ ($\Pr[\cdot \mid \cdot]$) denotes the (conditional) probability of interest. For a finite set $\mathcal{V}$, $|\mathcal{V}|$ denotes the number of elements of $\mathcal{V}$.

A. CONDITIONAL VALUE AT RISK

This section introduces a risk measure to assess the tail values of the probability distribution. Let $X \in \mathbb{R}$ be a random variable.

Definition 1 (Conditional value at risk [37], [38]): For a given confidence level $\alpha \in [0, 1)$, the CVaR of the loss distribution associated with a random variable X is defined as

$$\mathrm{CVaR}^{\alpha}[X] := \mathrm{E}\left[X | X \geq \mathrm{VaR}^{\alpha}[X]\right], \ \alpha \in [0, 1), \tag{1}$$

where

$$\mathrm{VaR}^{\alpha}[X] := \min\{x \in \mathbb{R} \mid \Pr[X \leq x] \geq \alpha\}. \tag{2}$$

(1) and (2) indicate that the CVaR is the mean value of the $(1-\alpha)$-tail distribution of $\Pr[X]$. Fig. 1 shows the VaR and CVaR for X with a probability distribution function $p(x)$.

The CVaR cost can be computed by solving the following linear programming problem [37].

$$\begin{aligned} \underset{\gamma, \xi \in \mathbb{R}}{\text{minimize}} \quad & \gamma + \frac{1}{1-\alpha} \sum_{x_i} \Pr[X = x_i]\, \xi(x_i), \\ \text{subject to} \quad & x_i - \xi(x_i) \leq \gamma, \ \xi(x_i) \geq 0. \end{aligned}$$

Moreover, Rockafellar *et al.* [37], [38] show that the CVaR cost is a *coherent measure* of risk defined by Artzner *et al.* [39]. Form the properties of the *coherent measure*, the CVaR satisfies the subadditivity property.

$$\mathrm{CVaR}^{\alpha}[X_1 + X_2] \leq \mathrm{CVaR}^{\alpha}[X_1] + \mathrm{CVaR}^{\alpha}[X_2].$$

B. CHERNOFF's INEQUALITY AND ENTROPIC VALUE AT RISK

The inequality shown below is known as Chernoff's inequality.

Lemma 1 (Chernoff's Inequality [40]): For a given random variable X, constant x_0, and positive number $\lambda > 0$, the following inequality holds:

$$\Pr[X \geq x_0] \leq \frac{\mathrm{E}\left[\exp \lambda X\right]}{\exp \lambda x_0}.$$

Chernoff's inequality quantifies the tail probability of $X \geq x_0$ using high-order moments. This is because $\mathrm{E}\left[\exp \lambda X\right]$ is the definition of the moment-generating function that can be used to obtain the moments of the distribution.

In addition, we define the cumulant-generating function.

Definition 2 (Cumulant-Generating Function [41]): For a given positive number $\lambda > 0$, the cumulant-generating function of X is defined as

$$\Psi_X(\lambda) := \log\left(\mathrm{E}\left[\exp \lambda X\right]\right), \ \lambda > 0. \tag{3}$$

The cumulants can evaluate the high-order centered moments of X weighed by the parameter λ. The cumulant-generating function holds the following linear property for the independent random variables X_1, X_2.

$$\Psi_{(X_1+X_2)}(\lambda) = \Psi_{X_1}(\lambda) + \Psi_{X_2}(\lambda). \tag{4}$$

Chernoff's inequality yields the following upper bound of the VaR by solving $\exp -\lambda x_0 \mathrm{E}\left[\exp \lambda X\right] = \alpha$ for x_0.

$$x_0(\alpha, \lambda) := \frac{1}{\lambda} \log\left(\frac{\mathrm{E}\left[\exp \lambda X\right]}{1-\alpha}\right). \tag{5}$$

By tightening the upper bound, we introduce another *coherent risk measure*.

Definition 3 (Entropic Value at Risk [42]): For a given confidence level $\alpha \in [0, 1)$, the EVaR of the loss distribution associated with a random variable X is defined as

$$\begin{aligned} \mathrm{EVaR}^{\alpha}[X] &:= \inf_{\lambda > 0} \frac{1}{\lambda} \log\left(\frac{\mathrm{E}\left[\exp \lambda X\right]}{1-\alpha}\right) \\ &= \inf_{\lambda > 0} \frac{1}{\lambda} \Psi_X(\lambda) - \frac{1}{\lambda} \log(1-\alpha), \end{aligned}$$

where $\Psi_X(\cdot)$ is the cumulant-generating function defined in (3).

Fig. 1 shows the EVaR and reveals the relationship $\mathrm{VaR}^{\alpha}[X] \leq \mathrm{CVaR}^{\alpha}[X] \leq \mathrm{EVaR}^{\alpha}[X]$. This inequality generally holds [42]. This relationship indicates that the EVaR is more conservative than the CVaR in evaluating the upper bound of the VaR for a random variable. However, the EVaR has a better property for the sum of independent random variables because of the linearity of the cumulant-generating function [42]. This property motivated us to use EVaR for the main result.

III. PROBLEM STATEMENTS AND MODELING

The objective of this paper is to minimize fuel consumption while enforcing a battery capacity constraint on the driving route. To achieve this, the method optimizes the drive mode switching depending on vehicle speeds based on the driving route and vehicle modeling described in Sections III-A and III-B.

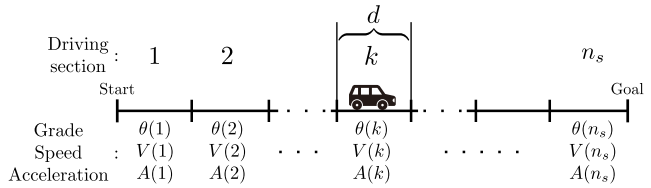

FIGURE 2. Driving-route modeling: $\theta(k)$ is the road grade (deterministic), $V(k)$ and $A(k)$ are the random variables of the vehicle speed and acceleration, respectively, and d is the distance of the driving sections.

Given the confidence level α, $p_c \in [0, 1)$ and a coefficient $\beta \in [0, 1]$, we examine the following risk-aware energy management problem:

$$\underset{U_i}{\text{minimize}} \quad (1-\beta)\mathrm{E}\left[\sum_i w_{\mathrm{f}}(X_i, U_i)\right] + \beta\,\mathrm{CVaR}^{\alpha}\left[\sum_i w_{\mathrm{f}}(X_i, U_i)\right], \tag{5a}$$

$$\text{subject to:} \quad \Pr\left[\sum_i w_{\mathrm{e}}(X_i, U_i) \geq q_r(k)\right] \leq 1 - p_c, \quad X_i \in \mathcal{X},\ U_i \in \mathrm{EV, HV}. \tag{5b}$$

This optimization is a discrete-type stochastic optimal drive mode control problem. The index i represents the number of discretized driving sections. $w_{\mathrm{f}}(\cdot,\cdot)$ and $w_{\mathrm{e}}(\cdot,\cdot)$ denote fuel and electricity demand functions, respectively. $q_r(k)$ is the remaining energy of the battery. $\mathcal{X}$ is a set of factors affecting a vehicle's energy requirement and element $X_i \in \mathcal{X}$ can be a random variable. U_i is the input that determines the PHEV drive modes. The cost function (5a) is the weighted mean and CVaR of fuel consumption. Risk awareness is adjusted by the confidence level α and the weight parameter β. The stochastic constraint (5b) requires that the probability of depleting the battery charge is less than or equal to $(1 - p_c)$. The constraint also evaluates the risk of electricity demand using the confidence level p_c. The remainder of this section presents the modeling for constructing the optimization problem (5) in detail. Furthermore, because (5) is an abstract form, a computationally tractable form is discussed in Section IV as the main result.

A. DRIVING-ROUTE MODELING

This paper introduces the finite and discretized driving route model shown in Fig. 2. Each discretized section of the route is assigned numbers $1, 2, \ldots, n_s$, and the sampling distance d is constant. In Fig. 2, $\theta(k)$ denotes the road grade, and $V(k)$ and $A(k)$ denote discrete random variables of vehicle speed and acceleration, respectively, in each driving section. Suppose that the driving route is estimated in advance, e.g., a commuter driving and a driving route navigated by systems. In addition, the following assumptions are made:

Assumption 1: The road grade $\theta(k)$ is a deterministic variable. The discrete random variables $V(k)$ and $A(k)$ have possible values of $\mathcal{V} := \{v_1, v_2, \ldots, v_{|\mathcal{V}|}\}$ and $\mathcal{A} := \{a_1, a_2, \ldots, a_{|\mathcal{A}|}\}$, respectively.

The road grade can be obtained using network services, such as the global positioning system and terrain maps. Vehicle speed $V(k)$ follows a discrete conditional probability distribution with the Markov property:

$$\Pr\left[V(k+1) = v' \mid V(k) = v\right] \geq 0,\ v, v' \in \mathcal{V}, \quad \sum_{v' \in \mathcal{V}} \Pr\left[V(k+1) = v' \mid V(k) = v\right] = 1, \tag{6}$$

and we define the transition probability matrices $\Pi_V(k)$, whose (j_v, j_v')-th entry is given by

$$[\Pi_V(k)]_{j_v j_v'} := \Pr\left[V(k+1) = v_{j_v'} \mid V(k) = v_{j_v}\right],$$

$j_v, j_v' \in \{1, 2, \ldots, |\mathcal{V}|\}$. We assume that the initial probability distribution $\Pr[V(1)]$ is known. In addition, the vehicle acceleration $A(k)$ follows the following discrete conditional probability distribution:

$$\Pr[A(k) = a \mid V(k) = v] \geq 0,\ a \in \mathcal{A},\ v \in \mathcal{V}, \quad \sum_{a \in \mathcal{A}} \Pr[A(k) = a \mid V(k) = v] = 1. \tag{7}$$

Assumption 2: At the current distance section $k \in \{1, 2, \ldots, n_s - 1\}$, the realization of the vehicle speed $v(k) \in \mathcal{V}$ and the value of the state of charge (SoC) of the battery $soc(k) \in [0, 1]$ are known.

The conditional probability distributions of the speed (6) and acceleration (7) can be estimated from the driving cycle data. This paper employs a simple estimation based on the Nadaraya–Watson kernel regression [43], [44] and Gaussian functions. Fig. 3 shows an estimated transition probability matrix and probability distributions of vehicle speed throughout a trip. The probability distributions in Fig. 3b can be calculated using the estimated transition matrices Π_V as

$$\Pr[V(i)] = \Pr[V(i-1)]\,\Pi_V(i),\ i \in \{k+1, \ldots, n_s\},$$

where

$$\Pr[V(i)] = \left[\Pr[V(i) = v_1] \cdots \Pr\left[V(i) = v_{|\mathcal{V}|}\right]\right],$$

$$\Pr[V(k)] = \left[\mathrm{I}[v(k) = v_1] \cdots \mathrm{I}\left[v(i) = v_{|\mathcal{V}|}\right]\right],$$

and the Markov property is used. $\mathrm{I}[\cdot]$ is the indicator function of $[\cdot]$, i.e., $\mathrm{I}[\cdot] = \{1 : \text{if } [\cdot] \text{ is true},\ 0 : \text{otherwise}\}$.

Fig. 4 depicts four example plots of vehicle speed versus acceleration at each driving section. By using collected data such as in Fig. 4, the conditional probabilities of acceleration (7) are also estimated using the Nadaraya–Watson method and speed probability distributions.

B. VEHICLE MODELING WITH ENERGY MAPS

This section outlines the vehicle modeling used to calculate the energy consumption and provides two energy maps. First, we define the control input $u(k, V(k))$ as the drive mode

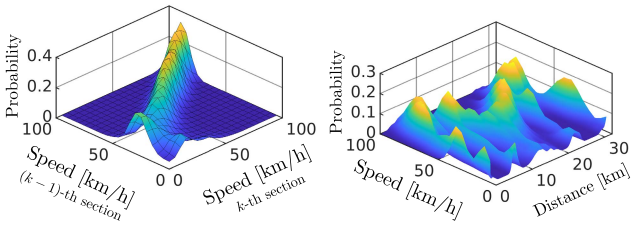

(a) Estimated transition probability matrix of vehicle speed at a pair of driving sections

(b) Probability distributions of vehicle speed throughout a trip

FIGURE 3. Stochastic modeling of vehicle speed on one driving route: The sampling distance intervals range from 0 to 32.1 km in increments of 0.1 km.

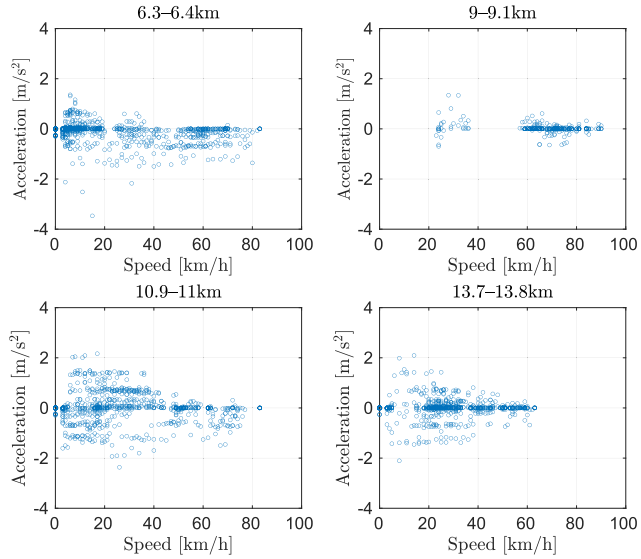

FIGURE 4. Relationship between speed and acceleration at some sections on a driving route: The measured data is used to estimate the conditional probability of the acceleration (7).

of a function of vehicle speed $V(k)$ at each driving section $k \in \{1, 2, \ldots, n_s\}$. Drive modes are classified into two types: electric-vehicle (EV) and hybrid-vehicle (HV) modes. The control input is expressed as a vector with respect to the discrete random variable of the vehicle speed $V(k)$ as follows:

$$u\left(k, V(k)\right) = \left[u\left(k, v_1\right), u\left(k, v_2\right), \ldots, u\left(k, v_{|\mathcal{V}|}\right)\right]^{\mathsf{T}}, \quad u\left(k, v_{j_v}\right) \in \{0, 1\}.$$

The modeling assumptions for the drive mode operation are as follows. These assumptions are based on the allocation strategy of the powertrain system implemented in the *Prius PHV* (2012 model). In the EV mode ($u\left(k, v_{j_v}\right) = 1$), the electric motor provides all the power required by the driver, and the engine is turned off. In the HV mode ($u\left(k, v_{j_v}\right) = 0$), the engine and electric machines supply the driving force while maintaining a constant SoC of the battery; the engine mainly generates the required power. In addition, the regenerated energy sourced from the brakes is consumed to re-accelerate the vehicle.

Let us assume that the lateral dynamics of a vehicle are sufficiently small for energy management. The longitudinal force f_{req} of the vehicle is obtained from Newton's second law of motion as

$$f_{\text{req}} = \frac{1}{2} c_D \rho_a h_a v^2 + \mu_{rr} v m g \cos\theta + \mu m g \sin\theta + m a, \quad (8)$$

where m is the vehicle mass, g is the acceleration of gravity, c_D is the aerodynamic drag resistance, ρ_a is the air density, h_a is the vehicle's frontal area, μ_{rr} is the rolling resistance coefficient, and μ is the coefficient of friction. θ, v, and a are provided along the driving route model. Let us now recall the assumptions of the driving modes. The torque demand for each condition (θ, v, a) can be divided into the engine and electric motor cases. Hence, to achieve the required force f_{req} at speed v, the PHEV must generate the following power for each drive mode.

$$w_{\text{f}}(\theta, v, a) = \eta_{\text{f}}\left(f_{\text{req}}, v\right) \cdot f_{\text{req}} v, \quad (9)$$

$$w_{\text{e}}(\theta, v, a) = \eta_{\text{e}}\left(f_{\text{req}}, v\right) \cdot f_{\text{req}} v, \quad (10)$$

where η_{f} and η_{e} denote the energy conversion efficiency of fuel in the HV mode and electricity in the EV mode, respectively.

To simplify the calculation of the required power (9) and (10), this study directly built two energy consumption maps $w_{\text{f}}(\theta, v, a)$, $w_{\text{e}}(\theta, v, a)$ depending on the discretization of the driving-route model. Fig. 5 depicts the identified energy consumption maps of fuel $w_{\text{f}}(\theta, v, 0)$ and electricity $w_{\text{e}}(\theta, v, 0)$ for $a = 0$ m/s^2. In Fig. 5, these maps are discretized at road grades of $-6, -5, \ldots, 6$ %, vehicle speeds of $5, 10, \ldots, 100$ km/h, and vehicle accelerations of $-4.00, -3.95, \ldots, 4.00$ m/s^2. The values of the maps are the average required power for the engine and battery under each discretized condition. The vehicle parameters in (8) are the same as those for the *Toyota Prius* model in ADVISOR [36] except for battery specifications. The battery specifications are adjusted to those of the actual *Toyota Prius PHV* (2012 model) [45] as shown in Table 1. The other structures and parameters remain at the default settings of the simulator. In other words, the detailed PHEV model of this study can be reproduced by reflecting only the values in Table 1. Note that the energy consumption maps are computed using the simulation results of ADVISOR. In practical cases, we can obtain a static map using pre-experimental data and vehicle specifications.

TABLE 1. Battery Specifications of the Prius PHV (2012 model) [45].

Cell voltage	3.7 V	Total voltage	207.2 V
Cell capacity	21.5 Ah	Total capacity	4.4 kWh
Number of cells	56	High SoC constraint	0.85
		Low SoC constraint	0.23

IV. RISK-AWARE ENERGY MANAGEMENT FOR DRIVE MODE SWITCHING

This section proposes risk-aware energy management for drive mode switching based on (5). The optimization problem in (5) is not computationally tractable from nonlinearity owing to the CVaR evaluation and stochastic constraint.

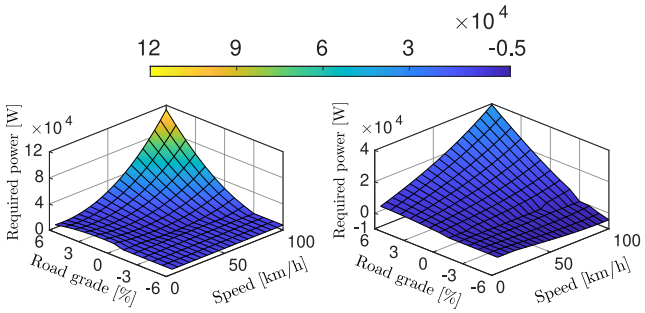

(a) Fuel in HV mode $w_{\mathrm{f}}(\theta, v, 0)$

(b) Electricity in EV mode $w_{\mathrm{e}}(\theta, v, 0)$

FIGURE 5. Vehicle modeling of a PHEV as two energy consumption maps $w_{\mathrm{f}}(\theta, v, a)$, $w_{\mathrm{e}}(\theta, v, a)$ based on the required force (8) and vehicle speed v: These maps were obtained from a detailed numerical simulator in this study.

We redefine the problem (5) as an MIECP problem in tractable form by exploiting the risk measure (CVaR and EVaR) properties. The solution to the MIECP problem subsequently determines the threshold value of the vehicle speed for switching the EV and HV modes on each driving section.

A. COST FUNCTION

Let $k \in \{1, 2, \ldots, n_s\}$ be the current number of driving sections on the driving route. We consider the following cost function combined with the mean value and CVaR of fuel consumption on the route.

$$\varphi_{\alpha,\beta} = (1-\beta)\,\mathrm{E}_V\left[\sum_{i=k+1}^{n_s} \widetilde{w}_{\mathrm{f}}(\theta(i), V(i))\overline{u}(i, V(i))\right] + \beta\,\mathrm{CVaR}_V^{\alpha}\left[\sum_{i=k+1}^{n_s} \widetilde{w}_{\mathrm{f}}(\theta(i), V(i))\overline{u}(i, V(i))\right], \quad (11)$$

where $\overline{u}(i, V(i)) := 1 - u(i, V(i))$, $\beta \in [0, 1]$ is a design parameter, and

$$\begin{aligned}&\widetilde{w}_{\mathrm{f}}(\theta(i), V(i))\\ &= \frac{\mathrm{E}_{A(i)}\left[w_{\mathrm{f}}(\theta(i), V(i), A(i))|V(i)\right]}{V(i)}d\\ &= \frac{d}{V(i)}\sum_{a_{j_a}\in\mathcal{A}} \Pr\left[A(i) = a_{j_a} \mid V(i)\right] w_{\mathrm{f}}(\theta(i), V(i), a_{j_a}).\end{aligned} \quad (12)$$

$\mathrm{E}_V[\cdot]$ and $\mathrm{CVaR}_V^{\alpha}[\cdot]$ denote the expected value and CVaR cost operators, respectively, for the random variables of the vehicle speed $V(i)$, $i \in \{k+1, k+2, \ldots, n_s\}$. From the structure of the cost function (11), the weight β can design the risk awareness of control performance. The weighting factor β increases and a risk-aware optimal solution reduces the spread of the fuel usage distribution measured by the CVaR.

The cost function (11) is derived directly from (5a) by employing the fuel consumption map $w_{\mathrm{f}}(\theta, v, a)$. Note that the form of (11) is not a linear cost function because the CVaR of the sum of random variables is involved. We then consider a linear function that provides an upper bound on the cost function (11).

Using the linearity of the expectation and subadditivity of the CVaR cost, we can transform the first and second terms of (11) as follows:

$$\begin{aligned}&\mathrm{E}_V\left[\sum_{i=k+1}^{n_s} \widetilde{w}_{\mathrm{f}}(\theta(i), V(i))\overline{u}(i, V(i))\right]\\ &= \sum_{i=k+1}^{n_s} \mathrm{E}_{V(i)}\left[\widetilde{w}_{\mathrm{f}}(\theta(i), V(i))\overline{u}(i, V(i))\right], \quad (13)\\ &\mathrm{CVaR}_V^{\alpha}\left[\sum_{i=k+1}^{n_s} \widetilde{w}_{\mathrm{f}}(\theta(i), V(i))\overline{u}(i, V(i))\right]\\ &\le \sum_{i=k+1}^{n_s} \mathrm{CVaR}_{V(i)}^{\alpha}\left[\widetilde{w}_{\mathrm{f}}(\theta(i), V(i))\overline{u}(i, V(i))\right]. \quad (14)\end{aligned}$$

From (13) and (14), the transformed cost function is defined as

$$\begin{aligned}\breve{\varphi}_{\alpha,\beta} = (1-\beta)&\sum_{i=k+1}^{n_s} \mathrm{E}_{V(i)}\left[\widetilde{w}_{\mathrm{f}}(\theta(i), V(i))\overline{u}(i, V(i))\right]\\ &+ \beta\sum_{i=k+1}^{n_s} \mathrm{CVaR}_{V(i)}^{\alpha}\left[\widetilde{w}_{\mathrm{f}}(\theta(i), V(i))\overline{u}(i, V(i))\right].\end{aligned} \quad (15)$$

The transformed cost function $\breve{\varphi}_{\alpha,\beta}$ is the upper bound of $\varphi_{\alpha,\beta}$. Thus, the proposed method aims to determine near-optimal inputs by minimizing the upper bound of (11).

B. STOCHASTIC CONSTRAINTS

The proposed method imposes the following stochastic constraints on the SoC of the battery:

$$\Pr\left[\sum_{i=k+1}^{n_s} \widetilde{w}_{\mathrm{e}}(\theta(i), V(i))u(i, V(i)) \ge q_r(k)\right] \le 1 - p_c, \quad (16)$$

where $\widetilde{w}_{\mathrm{e}}(\theta(i), V(i))$ is defined in the same manner as (12), p_c is a given confidence level parameter, $q_r(k) := q_{\mathrm{full}}(soc(k) - soc_{\min})$, and q_{full} is the total capacity of the battery. Note that (16) does not limit the maximum battery charge. To prevent overcharging, we can similarly construct a stochastic constraint.

The parameter p_c is determined by the designer according to the requirements for the desired fuel economy and battery constraints. For instance, if the designer sets the parameter $p_c = 0.5$, the controller subject to (16) depletes the SoC of the battery with a probability of less than 0.5. The design process also influences the fuel loss. An intuitive understanding

of this parameter was verified in the numerical simulations (Section V-B).

The remainder of this section introduces an approximated form of (16) that enables convex optimization. The stochastic constraint (16) cannot be straightforwardly supported by numerical optimization solvers. To overcome this difficulty, we convert the stochastic condition (16) into a deterministic form using Chernoff's inequality [40]. Therefore, this section presents theorems to derive sufficient conditions for the deterministic form.

Proposition 1: If (17) holds for the independent random variables $\widetilde{W}_{\mathrm{e}}(i) := \widetilde{w}_{\mathrm{e}}(\theta(i), V(i))u(i, V(i))$*, then the stochastic constraint (17) is satisfied.*

$$\sum_{i=k+1}^{n_s} \Psi_{\widetilde{W}_{\mathrm{e}}(i)}(\lambda) - \log(1-p_c) \leq \lambda q_r(k), \tag{17}$$

where $\lambda > 0$ *is a design parameter.*

Proof: The proof is provided in Appendix A. □

The cumulant-generating function in (17) involves high-order statistics, e.g., the second- and third-order centered moments. Hence, the deterministic constraint evaluates the risk of the SoC depletion.

The designer can tune the sensitivity to risk using the parameter λ. However, we cannot recognize the conservativeness of (17) until the optimization problem is solved. The next section presents a framework that optimizes λ by minimizing the left-hand side of (17). This approach adapts the method of determining the EVaR introduced in Definition 3. The framework is subsequently combined with the fuel-usage minimization problem.

C. CONSTRAINT REDESIGN WITH A DISCIPLINED CONVEX PROGRAMMING FRAMEWORK

In this section, the constraint (17) is redesigned with a disciplined convex programming framework based on [46]. The framework optimizes parameter λ and tightens the bound of the sufficient condition on (16). The redesigned constraint and risk-aware fuel evaluation (15) are formulated as the main optimization problem.

We first introduce an exponential cone [47], which is a convex set. The exponential cone is used to model various constraints involving exponentials and logarithms.

Definition 4 (Exponential Cone [47]): The (three-dimensional) exponential cone is defined as

$$K_{\exp} = (a,b,c) \mid b > 0,\ c \geq b\exp(\frac{a}{b}) \cup (a,b,c) \mid a \leq 0,\ b = 0,\ c \geq 0.$$

We then explain a lemma to demonstrate the proposed MIECP formulation. The problem of minimizing the left-hand side of (17) with λ is formulated as follows:

Lemma 2: Consider the constraint given by (17) with confidence level $p_c \in [0,1)$*. Let* $z = \frac{1}{\lambda}$*; subsequently, the minimization of the left-hand side of (17) by the parameter* z *is equivalent to*

$$\begin{aligned}
\underset{u_i,z,r_i,\zeta_i}{\text{minimize}} \quad & \sum_{i=k+1}^{n_s} r_i - z\log p_c, \\
\text{subject to:} \quad & z \geq \sum_{j_v=1}^{|\mathcal{V}|} \Pr\left[V(i) = v_{j_v}\right]\ \zeta_i(v_{j_v}), \\
& \left(\widetilde{w}_{\mathrm{e}}(\theta(i), v_{j_v})u(i, v_{j_v}) - r_i,\ z,\ \zeta_i(v_{j_v})\right) \in K_{\exp}, \\
& u(i, v_{j_v}) \in 0, 1, \\
& \forall v_{j_v} \in \mathcal{V},\ i \in \{k+1, \ldots, n_s\},
\end{aligned} \tag{18a}$$

where r_i *and* ζ_i *are the additional decision variables.*

Proof: The proof is provided in Appendix B. □

Remark 1: Note that the cost function (18a) is

$$\min_{u_i,z,r_i,\zeta_i} \sum_{i=k+1}^{n_s} r_i - z\log p_c = \mathrm{EVaR}^{p_c}_{V(i)}\left[\sum_{i=k+1}^{n_s} \widetilde{W}_{\mathrm{e}}(i)\right],$$

because $z = \frac{1}{\lambda}$ *is optimized for all* $i \in k+1, \ldots, n_s$*. The EVaR of the sum of* $\widetilde{W}_{\mathrm{e}}(i)$ *can be obtained exactly using the property of the cumulant-generating function. This is an advantage compared with the CVaR case because computing its CVaR is complicated.*

Because the left-hand side of (17) can be tightened by minimizing (18a), we rewrite the risk-aware energy management problem as a one-stage optimization problem.

Theorem 1: If Assumptions 1 and 2 hold, the following optimization problem satisfies the stochastic constraint (16).

$$\underset{u_i,z,r_i,\zeta_i}{\text{minimize}} \quad (15). \tag{19a}$$

$$\begin{aligned}
\text{subject to:} \quad & \sum_{i=k+1}^{n_s} r_i - z\log p_c \leq q_r(k), \\
& z \geq \sum_{j_v=1}^{|\mathcal{V}|} \Pr\left[V(i) = v_{j_v}\right]\ \zeta_i(v_{j_v}), \\
& \left(\widetilde{w}_{\mathrm{e}}(\theta(i), v_{j_v})u(i, v_{j_v}) - r_i,\ z,\ \zeta_i(v_{j_v})\right) \in K_{\exp}, \\
& u(i, v_{j_v}) \in 0, 1, \\
& \forall v_{j_v} \in \mathcal{V},\ i \in \{k+1, \ldots, n_s\}.
\end{aligned} \tag{19b}$$

Proof: The proof is derived from Proposition 1 and Lemma 2. □

Because the cost function (15) only evaluates the fuel usage, a solver makes the left-hand side of (19b) as small as possible. This tightening process corresponds to Lemma 2; thus, the optimal solution of (19) satisfies

$$\mathrm{EVaR}^{p_c}_{V(i)}\left[\sum_{i=k+1}^{n_s} \widetilde{W}_{\mathrm{e}}(i)\right] \leq q_r(k). \tag{19b*}$$

From this perspective, the proposed method simultaneously solves the two optimization problems as a one-stage optimization problem.

Remark 2: Recall the inequality $\mathrm{CVaR}^{\alpha}[X] \leq \mathrm{EVaR}^{\alpha}[X]$ *for a random variable* X *and confidence level* $\alpha \in [0, 1)$. *It may be better to evaluate the CVaR to reduce the conservativeness of the sufficient condition on (16). However,* $\mathrm{CVaR}^{\alpha}\left[\sum_i X(i)\right]$ *cannot be computed directly in a convex optimization manner, such as the EVaR in (19).*

The optimization problem (19) is solved for every driving section by updating the vehicle speed $v(k)$ and SoC $soc(k)$, similar to the MPC approach. Here, the optimization has the following property:

Corollary 1: The optimization problem (19) is recursively feasible in any driving section $k \in \{0, \ldots, n_s - 1\}$.

Proof: The proof is to show that the worst case $u(i, v_{j_v}) = 0,\ \forall i,\ \forall v_{j_v} \in \mathcal{V}$ for the cost function (15) is a feasible solution to the constraints of (19). For example, because the exponential cone $K_{\exp}$ and $q_r \geq 0$ contains a set $(a, b, c) \mid a \leq 0,\ b = 0,\ c \geq 0$, the case $z = r_i = \zeta_i = 0,\ \forall i \in k+1, \ldots, n_s$ is feasible for the worst solution. □

Remark 3: This feasibility is one of the motivations for using a disciplined convex programming framework. If (17) is directly adopted as a constraint, such an optimization problem can be infeasible.

V. NUMERICAL SIMULATIONS WITH REAL-WORLD DATA

Numerical validations were demonstrated using ADVISOR [36] with real-world driving cycles. This study employed MOSEK [48] as the MIECP problem solver. The simulations were executed on a standard computer with an AMD Ryzen 9 3900X CPU @ 3.80 GHz and 32 GB of RAM using Ubuntu desktop OS.

This study demonstrated the proposed mode-switching method using commuter and research driving data. The commuting route labeled *Route-A* was a real-world suburban route with a total 32.1 km trip and a road grade profile in Fig. 6. The driving data for research labeled *Route-B* were measured in the experiments of [49]. The road grade of Route-B is shown in Fig. 7, which was obtained using the method in [50]. The transition probability matrices ($\mathcal{V} = 5, 10, \ldots, 100$, *i.e.*, $|\mathcal{V}| = 20$) on Route-A and Route-B were estimated with 60 and 20 cycle profiles, respectively. To validate the proposed method, we studied 100 (Route-A) and 10 (Route-B) real cycle profiles. The studied profiles did not include profiles for predicting transition probabilities.[2]

In this simulation, we considered adding a heuristic constraint to conduct a study for practical use, as follows:

$$u\left(i, v_{j_v}\right) \geq u\left(i, v_{j'_v}\right) \text{ where } v_{j_v} < v_{j'_v},\ v_{j_v}, v_{j'_v} \in \mathcal{V}. \quad (20)$$

This heuristic constraint (20) transforms the drive mode-switching problem for each vehicle speed $v \in \mathcal{V}$ into a problem at a vehicle speed threshold $v_{\mathrm{th}} \in \mathcal{V}$. The transformation reduces computational costs and controls the data packets sent to the PHEV. Note that constraint (20) does not affect Theorem 1.

[2]Informed consent is obtained for the driving cycle data, and this study is approved by the relevant research ethics committee.

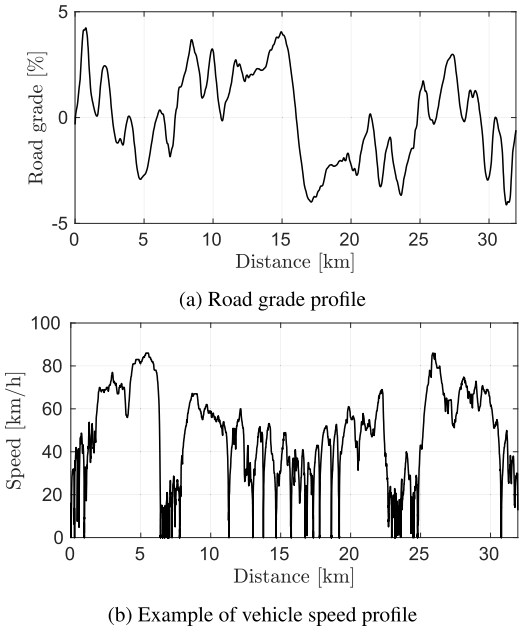

(a) Road grade profile

(b) Example of vehicle speed profile

FIGURE 6. Driving information for Route-A (commuter driving).

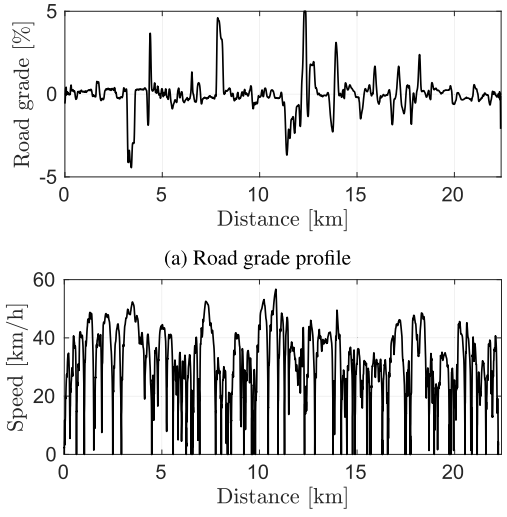

(a) Road grade profile

(b) Example of vehicle speed profile

FIGURE 7. Driving information for Route-B (driving study data [49], [50]).

The average computation time required to solve (19) was a few minutes. With this computation time, the optimization of each driving section could not be completed in real time. Several relaxations of binary optimization can be used to reduce the complexity of practical implementations. This study focused on the properties of the optimization-based controller (19), and computational burden reduction is a topic for future research.

A. NUMERICAL ANALYSIS OF FUEL ECONOMY FOR RISK-AWARE DRIVE MODE SWITCHING

We investigated the control performance of the proposed method for the parameter β related to the CVaR value for the

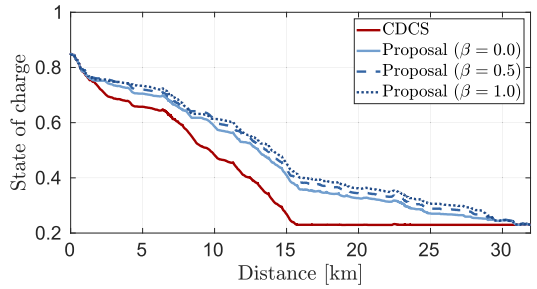

(a) SoC of the battery responses for the proposed and CDCS switching methods

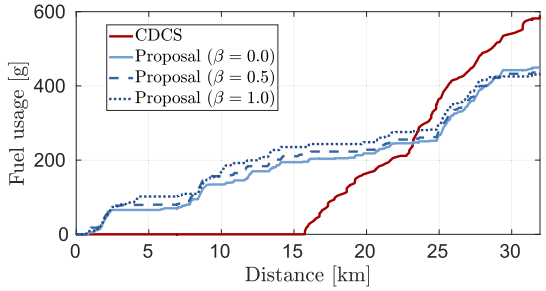

(b) Accumulated fuel consumption for the proposed and CDCS switching methods

FIGURE 8. Example of simulation results for Route-A.

cost function (15). The confidence level parameters were set as $\alpha = 0.5$ and $p_c = 0.5$. Fig. 8 shows an example of simulation results for Route-A. These graphs depict the accumulated fuel usage and SoC value history for each $\beta = 0.0, 0.5, 1.0$. This parametrization is to investigate if a risk-aware controller prevents unnecessary fuel consumption incidents by increasing the weight β. Fig. 9 summarizes the histograms of fuel usage for the CDCS and proposed methods.

The weight β of the CVaR cost increased, and the optimal solution was conservative. As a result, as shown in Fig. 8a, the proposed method with $\beta = 1.0$ sustained the SoC of the battery better than the other methods. As shown in Fig. 9, as the weight β increased, the distribution of fuel consumption shifted toward lower values. Similar results were obtained for Route-B. Tables 2 and 3 summarizes the average and 75th percentile fuel consumption improvement of the proposed method for $\beta = 0.0, 0.5, 1.0$ with the CDCS method. The results showed that the CVaR cost can quantify and control the tail of the fuel usage distribution. Furthermore, the parameter design regarding the CVaR cost can also affect the average fuel economy improvement from Table 2. For Route-B in Table 3, the case $\beta = 0.5$ was the maximum improvement at 16.55%, and the result must be verified with more driving data. Note that the design method for α, β must be further discussed, because the average fuel efficiency may decline depending on the driving conditions by increasing β.

B. NUMERICAL ANALYSIS OF STOCHASTIC CONSTRAINTS BASED ON THE ENTROPIC VALUE AT RISK

The less conservative bound satisfying (16) indirectly decreases the cost function (15). This section numerically

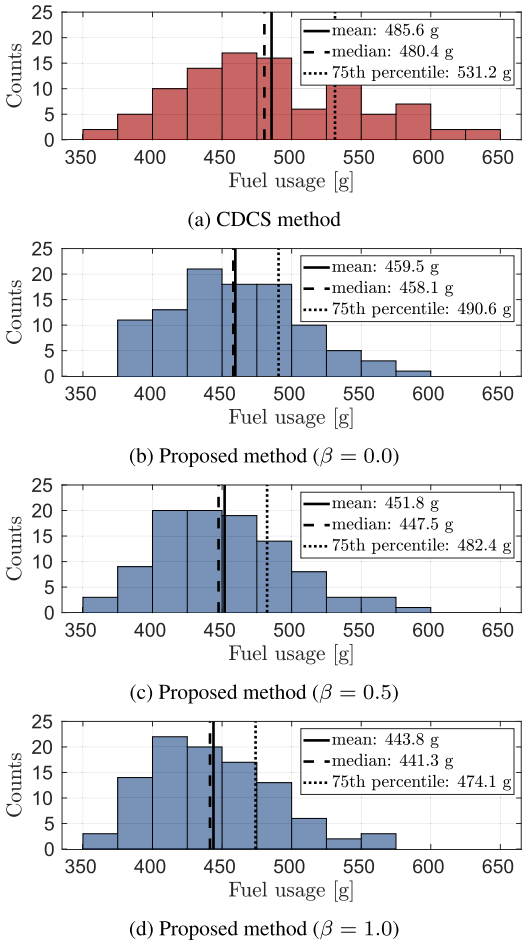

(a) CDCS method

(b) Proposed method ($\beta = 0.0$)

(c) Proposed method ($\beta = 0.5$)

(d) Proposed method ($\beta = 1.0$)

FIGURE 9. Fuel economy improvement at the 75th percentile of the proposed method for $\beta = 0.0, 0.5, 1.0$ on CDCS.

TABLE 2. Average fuel economy improvement of the proposed method for $\beta = 0.0, 0.5, 1.0$ on CDCS.

	$\beta = 0.0$	$\beta = 0.5$	$\beta = 1.0$
Route-A	5.36%	6.95%	8.60%
Route-B	12.57%	15.12%	16.09%

verifies the conservativeness of the SoC constraints with the EVaR bound (19b).

Note that the VaR, CVaR, and EVaR bounds for the sum of the random variables $\sum_{i=k+1}^{n_s} \widetilde{W}_e(i)$ have the following properties:

- A necessary and sufficient condition for the stochastic constraint (16) is that $\mathrm{VaR}_V^{p_c}\left[\sum_{i=k+1}^{n_s} \widetilde{W}_e(i)\right] \leq q_r(k)$ is satisfied.
- $\mathrm{VaR}_V^{p_c}\left[\sum_{i=k+1}^{n_s} \widetilde{W}_e(i)\right]$ and $\mathrm{CVaR}_V^{p_c}\left[\sum_{i=k+1}^{n_s} \widetilde{W}_e(i)\right]$ cannot be computed with a convex optimization problem straightforwardly.
- A tractable bound $\sum_{i=k+1}^{n_s} \mathrm{CVaR}_V^{p_c}\left[\widetilde{W}_e(i)\right]$ can be used as an upper bound of $\mathrm{CVaR}_V^{p_c}\left[\sum_{i=k+1}^{n_s} \widetilde{W}_e(i)\right]$ due to the subadditivity.
- $\mathrm{EVaR}_V^{p_c}\left[\sum_{i=k+1}^{n_s} \widetilde{W}_e(i)\right]$ is calculated with the disciplined optimization framework without approximation.

TABLE 3. Fuel economy improvement at the 75th percentile of the proposed method for $\beta = 0.0, 0.5, 1.0$ on CDCS.

	$\beta = 0.0$	$\beta = 0.5$	$\beta = 1.0$
Route-A	7.64%	9.19%	10.75%
Route-B	12.85%	16.55%	12.85%

Based on the above discussion, we introduce and compare the following values as conservativeness indices:

- CVaR bound:

$$\frac{\sum_{i=k+1}^{n_s} \mathrm{CVaR}_V^{p_c}\left[\widetilde{W}_\mathrm{e}(i)\right] - \mathrm{VaR}_V^{p_c}\left[\sum_{i=k+1}^{n_s} \widetilde{W}_\mathrm{e}(i)\right]}{q_\mathrm{full}}, \quad (21a)$$

- EVaR bound:

$$\frac{\mathrm{EVaR}_V^{p_c}\left[\sum_{i=k+1}^{n_s} \widetilde{W}_\mathrm{e}(i)\right] - \mathrm{VaR}_V^{p_c}\left[\sum_{i=k+1}^{n_s} \widetilde{W}_\mathrm{e}(i)\right]}{q_\mathrm{full}}, \quad (21b)$$

where we estimated $\mathrm{VaR}_V^{p_c}\left[\sum_{i=k+1}^{n_s} \widetilde{W}_\mathrm{e}(i)\right]$ with random samples using the optimized drive-mode inputs. The index (21) represents the excess of virtual SoC values when the proposed controller determines the drive modes with the optimization (19). The smaller the index is, the better the controller can select an input that reduces the cost function (15).

Fig. 10 depicts the conservativeness index (21) for $p_c = 0.2, 0.5, 0.8$ at each driving section $k \in 0, \ldots, n_s - 1$. First, the EVaR bounds were smaller than the CVaR bounds for all $p_c = 0.2, 0.5, 0.8$ and $k \leq 300$. Second, for the CVaR and EVaR with $p_c = 0.8$, at least 0.05 difference existed through the driving sections from 1 to 180. Note that while each conservativeness index reached almost the same value for the driving sections for $k \geq 300$, conservative optimization at $k = 1, \ldots, 180$ caused unnecessary fuel consumption. In other words, the CVaR upper bounds degrade controller performance if we employ the value for the battery constraint.

In the problem setting of this study, we numerically confirmed that the proposed method maintains a conservativeness index below 0.01 when $p_c \geq 0.5$. This result is beneficial because the designed confidence level p_c exceeds 0.5 in many applications. We conclude that the proposed method is useful because these numerical results were achieved through verification using real-world driving data. Note that, similar to the results for Route-A shown in Fig. 10, similar results for Route-B were observed, and we omit the details.

The risk evaluation results, such as Fig. 10, can also be numerically derived for numerous simple cases.[3] A mathematically rigorous analysis of the conservativeness of the EVaR bound ($\mathrm{EVaR}_V^{p_c}\left[\sum_{i=k+1}^{n_s} \widetilde{W}_\mathrm{e}(i)\right]$) is a future research direction.

[3]Assuming the random variables $\widetilde{W}_\mathrm{e}(i)$, $i = 1, 2, \ldots, n_s$ are independent and identically distributed random variables, we can numerically obtain many scenarios supporting the results shown in Fig. 10.

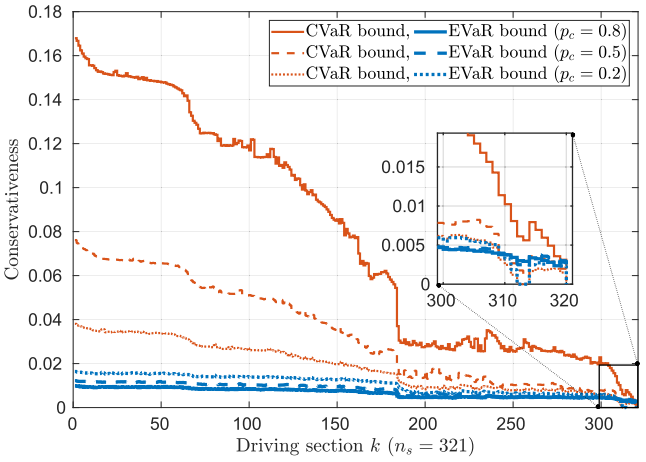

FIGURE 10. Conservativeness index values of the CVaR and EVaR bound defined in (21) for $p_c = 0.2, 0.5, 0.8$.

VI. CONCLUSION

This paper addresses the risk-aware energy management of the drive mode of PHEVs. The CVaR cost and EVaR bound constraint are introduced to quantify the risk of energy consumption. These measurements result in the formulation of an MIECP problem that determines the vehicle speed threshold value in the drive mode. Numerical simulations with real-world data investigated the effects of the design parameters for fuel economy and conservativeness on the optimization problem. The numerical simulations revealed that the high-weighted CVaR cost can prevent the spread of the fuel loss distribution in the positive direction. The designed controller achieved 8.60% and 16.09% improvements on average and 10.75% and 12.85% reductions at the 75th percentile compared with the CDCS method on two selected real-world routes. In addition, this validation indicated that the EVaR bound is computationally affordable and provides less conservative characteristics for the sum of random variables.

The proposed method was evaluated for two driving routes: commuter driving (Route-A) and research experiment driving (Route-B). Although each route had different characteristics in terms of energy consumption, this method improved the fuel economy. Addressing additional verification with a larger class of driving routes is essential because the simulation can clarify the driving route conditions that are applicable to the proposed method. Additional verification is required in future research. Section V presents the control performance characteristics by the weight parameters via the simulations with real-world data, but comprehensive design methodologies remain to be investigated.

APPENDIX A PROOF OF PROPOSITION 1

Proof: From Lemma 1, we obtain the following inequality:

$$\Pr\left[\sum_{i=k+1}^{n_s} \widetilde{W}_\mathrm{e}(i) \geq q_r(k)\right] \leq \frac{\mathrm{E}_V\left[\exp\lambda \sum_{i=k+1}^{n_s} W_\mathrm{e}(i)\right]}{\exp\lambda q_r(k)},$$

(22)

where $\widetilde{W}_{\mathrm{e}}(i) := \widetilde{w}_{\mathrm{e}}(\theta(i), V(i))u\,(i, V(i))$ is defined to simplify notation. Let the right-hand side of (22) be p_c, that is,

$$p_c = \frac{\mathrm{E}_V\left[\exp\lambda\sum_{i=k+1}^{n_s}\widetilde{W}_{\mathrm{e}}(i)\right]}{\exp\lambda q_r(k)}. \tag{23}$$

Substituting (23) into (22), we obtain

$$\Pr\left[\sum_{i=k+1}^{n_s}\widetilde{W}_{\mathrm{e}}(i) \geq \frac{1}{\lambda}\sum_{i=k+1}^{n_s}\Psi_{\widetilde{W}_{\mathrm{e}}(i)}(\lambda) - \frac{1}{\lambda}\log p_c\right] \leq p_c,$$

where the mutual independence of $\widetilde{W}_{\mathrm{e}}(i)$ is used. The above result indicates that if the following condition

$$\frac{1}{\lambda}\sum_{i=k+1}^{n_s}\Psi_{\widetilde{W}_{\mathrm{e}}(i)}(\lambda) - \frac{1}{\lambda}\log p_c \leq q_r(k)$$

is satisfied, the stochastic constraint (16) is fulfilled. □

APPENDIX B PROOF OF LEMMA 2

Proof: Let $\lambda = \frac{1}{z}$, $z > 0$. Thus, $\frac{1}{\lambda}\Psi_X(\lambda) = z\Psi_X(\frac{1}{z})$. From Definition 3 and the properties of the cumulant-generating function (4),

$$\begin{aligned}
&\mathrm{EVaR}_V^{p_c}\left[\sum_{i=k+1}^{n_s}\widetilde{W}_{\mathrm{e}}(i)\right] \\
&= \min_{z>0} z\,\Psi_{\sum_{i=k+1}^{n_s}\widetilde{W}_{\mathrm{e}}(i)}(\frac{1}{z}) - z\log p_c \\
&= \min_{z>0} z\sum_{i=k+1}^{n_s}\Psi_{\widetilde{W}_{\mathrm{e}}(i)}(\frac{1}{z}) - z\log p_c.
\end{aligned}$$

Considering $z\,\Psi_{\widetilde{W}_{\mathrm{e}}(i)}(\frac{1}{z})$ for $i \in k+1, \ldots, n_s$, we can express the perspective of the log-sum-exp function [51] as

$$\begin{aligned}
r_i &\geq z\,\Psi_{\widetilde{W}_{\mathrm{e}}(i)}(\frac{1}{z}), \\
0 &\geq \Psi_{\widetilde{W}_{\mathrm{e}}(i)}(\frac{1}{z}) - \log(\exp(\frac{r_i}{z})), \\
1 &\geq \mathrm{E}_V\left[\exp(\frac{\widetilde{W}_{\mathrm{e}}(i) - r_i}{z})\right], \\
z &\geq \mathrm{E}_V\left[z\exp(\frac{\widetilde{W}_{\mathrm{e}}(i) - r_i}{z})\right],
\end{aligned}$$

where r_i is the new decision variable. By introducing the additional decision variables $\zeta_i(v_{j_v})$, $v_{j_v} \in \mathcal{V}$, we can formulate

$$z \geq \sum_{j_v=1}^{|\mathcal{V}|}\Pr\left[V(i) = v_{j_v}\right]\,\zeta_i(v_{j_v}), \tag{24}$$

$$\zeta_i(v_{j_v}) \geq z\exp(\frac{\widetilde{w}_{\mathrm{e}}(\theta(i), v_{j_v})u(i, v_{j_v}) - r_i}{z}). \tag{25}$$

The inequality (25) is an exponential cone [47]

$$\begin{aligned}
\zeta_i(v_{j_v}) \quad &\geq \quad z\exp(\frac{\widetilde{w}_{\mathrm{e}}(\theta(i), v_{j_v})u(i, v_{j_v}) - r_i}{z}),\ z > 0 \\
&\iff \left(\widetilde{w}_{\mathrm{e}}(\theta(i), v_{j_v})u(i, v_{j_v}) - r_i, z, \zeta_i(v_{j_v})\right) \in K_{\exp}.
\end{aligned}$$

(26)

The minimization of the perspective of the log-sum-exp function for each $i \in k+1, \ldots, n_s$ is

$$\begin{aligned}
&\underset{u_i, z, r_i, \zeta_i}{\text{minimize}} \quad r_i \\
&\text{subject to:} \quad (24) \text{ and } (26).
\end{aligned}$$

From the above considerations, we can express the disciplined convex programming framework [52] of $\mathrm{EVaR}^{p_c}\left[\sum_{i=k+1}^{n_s}\widetilde{W}_{\mathrm{e}}(i)\right]$ as follows:

$$\begin{aligned}
&\mathrm{EVaR}_V^{p_c}\left[\sum_{i=k+1}^{n_s}\widetilde{W}_{\mathrm{e}}(i)\right] \\
&= \begin{cases}
\text{minimize}_{u,z,r,\zeta} & \sum_{i=k+1}^{n_s} r_i - z\log p_c \\
\text{subject to:} & (24) \text{ and } (26),\ i \in \{k+1, \ldots, n_s\}.
\end{cases}
\end{aligned}$$

This completes the proof of Lemma 2. □

ACKNOWLEDGMENT

The authors would like to thank Prof. Susumu Sato at the Tokyo Institute of Technology for providing the research data used in the numerical validation and also would like to thank Editage (www.editage.com) for English language editing.

REFERENCES

[1] S. G. Wirasingha and A. Emadi, "Classification and review of control strategies for plug-in hybrid electric vehicles," *IEEE Trans. Veh. Technol.*, vol. 60, no. 1, pp. 111–122, Jan. 2011.
[2] J. L. Torres, R. Gonzalez, A. Gimenez, and J. Lopez, "Energy management strategy for plug-in hybrid electric vehicles. A comparative study," *Appl. Energy*, vol. 113, pp. 816–824, Jan. 2014.
[3] C. M. Martinez, X. Hu, D. Cao, E. Velenis, B. Gao, and M. Wellers, "Energy management in plug-in hybrid electric vehicles: Recent progress and a connected vehicles perspective," *IEEE Trans. Veh. Technol.*, vol. 66, no. 6, pp. 4534–4549, Jun. 2016.
[4] G. Ripaccioli, D. Bernardini, S. Di Cairano, A. Bemporad, and I. V. Kolmanovsky, "A stochastic model predictive control approach for series hybrid electric vehicle power management," in *Proc. Amer. Control Conf.*, Jun. 2010, pp. 5844–5849.
[5] S. J. Moura, H. K. Fathy, D. S. Callaway, and J. L. Stein, "A stochastic optimal control approach for power management in plug-in hybrid electric vehicles," *IEEE Trans. Control Syst. Technol.*, vol. 19, no. 3, pp. 545–555, May 2011.
[6] S. Di Cairano, D. Bernardini, A. Bemporad, and I. V. Kolmanovsky, "Stochastic MPC with learning for driver-predictive vehicle control and its application to HEV energy management," *IEEE Trans. Control Syst. Technol.*, vol. 22, no. 3, pp. 1018–1031, May 2014.
[7] Y. Zhou, A. Ravey, and M.-C. Péra, "A survey on driving prediction techniques for predictive energy management of plug-in hybrid electric vehicles," *J. Power Sources*, vol. 412, pp. 480–495, Oct. 2019.
[8] P. Pisu and G. Rizzoni, "A comparative study of supervisory control strategies for hybrid electric vehicles," *IEEE Trans. Control Syst. Technol.*, vol. 15, no. 3, pp. 506–518, May 2007.
[9] A. Sciarretta, G. De Nunzio, and L. L. Ojeda, "Optimal ecodriving control: Energy-efficient driving of road vehicles as an optimal control problem," *IEEE Control Syst.*, vol. 35, no. 5, pp. 71–90, Oct. 2015.
[10] M. Vajedi and N. L. Azad, "Ecological adaptive cruise controller for plug-in hybrid electric vehicles using nonlinear model predictive control," *IEEE Trans. Intell. Transp. Syst.*, vol. 17, no. 1, pp. 113–122, Jan. 2015.
[11] L. Johannesson, M. Asbogard, and B. Egardt, "Assessing the potential of predictive control for hybrid vehicle powertrains using stochastic dynamic programming," *IEEE Trans. Intell. Transp. Syst.*, vol. 8, no. 1, pp. 71–83, Mar. 2007.

[12] V. Larsson, L. J. Mårdh, B. Egardt, and S. Karlsson, "Commuter route optimized energy management of hybrid electric vehicles," *IEEE Trans. Intell. Transp. Syst.*, vol. 15, no. 3, pp. 1145–1154, Jun. 2014.
[13] A. Furberg, V. Larsson, and B. Egardt, "Optimal selection of driving modes along a commuter route for a plug-in hybrid electric vehicle," *IFAC Proc. Volumes*, vol. 47, no. 3, pp. 7867–7872, 2014.
[14] A. A. Malikopoulos, "A multiobjective optimization framework for online stochastic optimal control in hybrid electric vehicles," *IEEE Trans. Control Syst. Technol.*, vol. 24, no. 2, pp. 440–450, Mar. 2016.
[15] C. Sun, S. J. Moura, X. Hu, J. K. Hedrick, and F. Sun, "Dynamic traffic feedback data enabled energy management in plug-in hybrid electric vehicles," *IEEE Trans. Control Syst. Technol.*, vol. 23, no. 3, pp. 1075–1086, May 2015.
[16] X. Qi, G. Wu, K. Boriboonsomsin, M. J. Barth, and J. Gonder, "Data-driven reinforcement learning–based real-time energy management system for plug-in hybrid electric vehicles," *Transp. Res. Rec., J. Transp. Res. Board*, vol. 2572, pp. 1–8, Jan. 2016.
[17] L. L. Guo, B. Gao, Y. Gao, and H. Chen, "Optimal energy management for HEVs in eco-driving applications using bi-level MPC," *IEEE Trans. Intell. Transp. Syst.*, vol. 18, no. 8, pp. 2153–2162, Aug. 2016.
[18] Y. Choi, J. Guanetti, S. Moura, and F. Borrelli, "Data-driven energy management strategy for plug-in hybrid electric vehicles with real-world trip information," in *Proc. 21st IFAC World Congr.*, 2020, pp. 14224–14229.
[19] C. Sun, J. Guanetti, F. Borrelli, and S. J. Moura, "Optimal eco-driving control of connected and autonomous vehicles through signalized intersections," *IEEE Internet Things J.*, vol. 7, no. 5, pp. 3759–3773, May 2020.
[20] Z. Zhu, N. Pivaro, S. Gupta, A. Gupta, and M. Canova, "Safe model-based off-policy reinforcement learning for eco-driving in connected and automated hybrid electric vehicles," *IEEE Trans. Intell. Vehicles*, vol. 7, no. 2, pp. 387–398, Jun. 2022.
[21] A. Pozzi, S. Bae, Y. Choi, F. Borrelli, D. M. Raimondo, and S. Moura, "Ecological velocity planning through signalized intersections: A deep reinforcement learning approach," in *Proc. 59th IEEE Conf. Decis. Control (CDC)*, Dec. 2020, pp. 245–252.
[22] R. Watanabe, H. Yoshioka, T. Ibuki, Y. Sakayanagi, and M. Sampei, "Online optimal mode control for plug-in hybrid vehicles based on driving routes," in *Proc. 21st IFAC World Congr.*, 2020, pp. 14135–14140.
[23] R. Watanabe, S. Hirate, T. Ibuki, Y. Sakayanagi, and M. Sampei, "Route-optimized drive mode switching control for plug-in hybrid vehicles: Controller design and experimental validation," in *Proc. IEEE Conf. Control Technol. Appl. (CCTA)*, Aug. 2020, pp. 207–212.
[24] C. W. Miller and I. Yang, "Optimal control of conditional value-at-risk in continuous time," *SIAM J. Control Optim.*, vol. 55, no. 2, pp. 856–884, Jan. 2017.
[25] J. R. Medina and S. Hirche, "Considering uncertainty in optimal robot control through high-order cost statistics," *IEEE Trans. Robot.*, vol. 34, no. 4, pp. 1068–1081, Aug. 2018.
[26] S. Singh, Y. Chow, A. Majumdar, and M. Pavone, "A framework for time-consistent, risk-sensitive model predictive control: Theory and algorithms," *IEEE Trans. Autom. Control*, vol. 64, no. 7, pp. 2905–2912, Jul. 2018.
[27] P. Sopasakis, M. Schuurmans, and P. Patrinos, "Risk-averse risk-constrained optimal control," in *Proc. 18th Eur. Control Conf. (ECC)*, Jun. 2019, pp. 375–380.
[28] M. Ahmadi, X. Xiong, and A. D. Ames, "Risk-averse control via CVaR barrier functions: Application to bipedal robot locomotion," *IEEE Control Syst. Lett.*, vol. 6, pp. 878–883, 2022.
[29] A. Dixit, M. Ahmadi, and J. W. Burdick, "Risk-sensitive motion planning using entropic value-at-risk," 2020, *arXiv:2011.11211*.
[30] N. Bäuerle and J. Ott, "Markov decision processes with average-value-at-risk criteria," *Math. Methods Oper. Res.*, vol. 74, no. 3, pp. 361–379, Dec. 2011.
[31] W. B. Haskell and R. Jain, "A convex analytic approach to risk-aware Markov decision processes," *SIAM J. Control Optim.*, vol. 53, no. 3, pp. 1569–1598, Jan. 2015.
[32] D. Jacobson, "Optimal stochastic linear systems with exponential performance criteria and their relation to deterministic differential games," *IEEE Trans. Autom. Control*, vol. AC-18, no. 2, pp. 124–131, Apr. 1973.
[33] F. Qian, J. Gao, and D. Li, "Complete statistical characterization of discrete-time LQG and cumulant control," *IEEE Trans. Autom. Control*, vol. 57, no. 8, pp. 2110–2115, Aug. 2011.
[34] K. D. Pham, *Linear-Quadratic Controls Risk-Averse Decision Making: Performance-Measure Statistics and Control Decision Optimization*. Cham, Switzerland: Springer, 2012.
[35] Z. Wu, S. Zhou, J. Li, and X.-P. Zhang, "Real-time scheduling of residential appliances via conditional risk-at-value," *IEEE Trans. Smart Grid*, vol. 5, no. 3, pp. 1282–1291, May 2014.
[36] A. Brooker, K. Haraldsson, T. Hendricks, V. Johnson, K. Kelly, B. Kramer, T. Markel, M. O'Keefe, S. Sprik, K. Wipke, M. Zolot, D. Bharathan, S. Burch, M. Cuddy, and D. Rausen. (2013) *Advisor -advanced vehicle simulator*. Accessed: Dec. 14, 2021. [Online]. Available: http://adv-vehicle-sim.sourceforge.net
[37] R. T. Rockafellar and S. Uryasev, "Optimization of conditional value-at-risk," *J. Risk*, vol. 2, pp. 21–42, Feb. 2000.
[38] R. Rockafellar and S. Uryasev, "Conditional value-at-risk for general loss distributions," *J. Banking Finance*, vol. 26, no. 7, pp. 1443–1471, Jul. 2002.
[39] P. Artzner, F. Delbaen, J.-M. Eber, and D. Heath, "Coherent measures of risk," *Math. Finance*, vol. 9, no. 3, pp. 203–228, Jul. 1999.
[40] S. Boucheron, G. Lugosi, and P. Massart, *Concentration Inequalities: A Nonasymptotic Theory of Independence*. Oxford, U.K.: Oxford Univ. Press, 2013.
[41] M. G. Kendall and A. Stuart, *The Advanced Theory of Statistics*, vol. 1, 3rd ed. London, U.K.: Charles Griffin and Co., 1969.
[42] A. Ahmadi-Javid, "Entropic value-at-risk: A new coherent risk measure," *J. Optim. Theory Appl.*, vol. 155, no. 3, pp. 1105–1123, Dec. 2012.
[43] E. A. Nadaraya, "On estimating regression," *Theory Probab. Appl.*, vol. 9, no. 1, pp. 141–142, 1964.
[44] G. S. Watson, "Smooth regression analysis," *Sankhyā, Indian J. Statist. A*, vol. 26, no. 4, pp. 359–372, 1964.
[45] Toyota Motor Corporation. (2016). *Toyota Prius PHV*. Accessed: Dec. 14, 2021. [Online]. Available: https://toyota.jp/pages/contents/priusphv/001_p_005/pdf/spec/priusphv_s%pec_201506.pdf
[46] D. Cajas, "Entropic portfolio optimization: A disciplined convex programming framework," Available SSRN 3792520, Feb. 2021.
[47] R. Chares, "Cones and interior-point algorithms for structured convex optimization involving powers and exponentials," Ph.D. dissertation, Louvain School Eng., Univ. Louvain, Louvain-la-Neuve, Belgium, 2009.
[48] MOSEK ApS. (2021) *Mosek*. Accessed: Dec. 14, 2021. [Online]. Available: https://www.mosek.com/
[49] S. Sato, H. Suzuki, M. Miya, and N. Iida, "Validation of CO_2 reduction effects and analysis of real-world emissions in eco-driving," *Trans. Soc. Automot. Eng. Jpn.*, vol. 43, no. 5, pp. 1145–1150, 2012.
[50] S. Sato, T. Yamamoto, Y. Ogawa, and N. Fukuro, "Research on measurement method of road gradient and altitude by on-road driving," *SAE Int. J. Fuels Lubricants*, vol. 2, no. 1, pp. 531–540, Apr. 2009.
[51] S. P. Boyd and L. Vandenberghe, *Convex Optimization*. Cambridge, U.K.: Cambridge Univ. Press, 2004.
[52] M. Grant, S. Boyd, and Y. Ye, "Disciplined convex programming," in *Global Optimization: From Theory to Implementation*, L. Liberti and N. Maculan, Eds. Cham, Switzerland: Springer, 2006, pp. 155–210.

RYUNOSUKE WATANABE (Member, IEEE) received the M.Eng. and Ph.D. degrees in systems and control engineering from the Tokyo Institute of Technology, in 2019 and 2022, respectively. His research interests include optimal control, optimization, and energy management and their applications.

TATSUYA IBUKI (Member, IEEE) received the B.Eng., M.Eng., and Ph.D. (Eng.) degrees from the Tokyo Institute of Technology, in 2008, 2010, and 2013, respectively. He was a Research Fellow with the Japan Society for the Promotion of Science, from 2012 to 2013, an Assistant Professor with the Department of Systems and Control Engineering, Tokyo Institute of Technology, from 2013 to 2020, and a Visiting Scholar with the School of Electrical and Computer Engineering, Georgia Institute of Technology, in 2019. Since 2020, he has been a Senior Assistant Professor with the Department of Electronics and Bioinformatics, School of Science and Technology, Meiji University. His research interests include the cooperative control of robotic networks, fusion of control theory and machine learning, and vision-based estimation and control.

YOSHIHIRO SAKAYANAGI received the M.Eng. and Ph.D. degrees from the Tokyo Institute of Technology, in 2000 and 2008, respectively. Since 2000, he has been with Toyota Motor Corporation, where he is currently a Researcher in powertrain control systems. His current research interests include connected vehicles and powertrain control systems.

RIKU FUNADA (Member, IEEE) received the B.Eng., M.Eng., and Ph.D. degrees from the Tokyo Institute of Technology, in 2014, 2016, and 2019, respectively. He was a Postdoctoral Researcher at Waseda University, in 2019, and the University of Texas at Austin, in 2020. He was also a Research Fellow of the Japan Society for the Promotion of Science, from 2016 to 2019. His research interests include cooperative control and networked robotics.

MITSUJI SAMPEI (Member, IEEE) received the B.Eng., M.Eng., and Dr.Eng. degrees in control engineering from the Tokyo Institute of Technology, in 1983, 1985, and 1987, respectively. From 1987 to 1993, he was a Research Associate and an Associate Professor at Chiba University. Since 1993, he has been with the Tokyo Institute of Technology, where he is currently a Professor with the Department of Systems and Control Engineering. His current research interests include nonlinear system theory, including under-actuated systems, nonholonomic systems, robotics, and H-infinity control theory. He served as an Organizing Committee Member at several conferences, including the IPC Chair of the IEEE Conference on Control Applications (CCA, 2010), the SICE Annual Conference (SICE 2011), and the IEEE Conference on Decision and Control (CDC 2015).